ENTROPY GENERATION ANALYSIS OF A SOLID OXIDE FUEL CELL BY COMPUTATIONAL FLUID DYNAMICS
Influence of Electrochemical Model and Its Parameters

by

Jose J. RAMIREZ-MINGUELA [a*], ***Juan M. MENDOZA-MIRANDA*** [b], ***Jose L. RODRIGUEZ-MUNOZ*** [c], ***Vicente PEREZ-GARCIA*** [c], ***Jorge A. ALFARO-AYALA*** [a], ***and Agustin R. URIBE-RAMIREZ*** [a]

[a] Department of Chemical Engineering, University of Guanajuato, Guanajuato, Gto., Mexico
[b] Interdisciplinary Professional Unit of Engineering Campus Guanajuat, National Polytechnic Institute, Silao de la Victoria, Gto., Mexico
[c] Department of Metal-Mechanics, Technological University of Southwest Guanajuato, Valle de Santiago, Gto., Mexico

Original scientific paper
https://doi.org/10.2298/TSCI151221127R

The aim of this paper is to evaluate numerically the effect of varying the electrochemical model and its parameters on the performance and entropy generation of a mono-block-layer build (MOLB) type geometry of a solid oxide fuel cell. Particularly, the influence of the exchange of current density, the electrical conductivity of the electrodes and the electrolyte has been studied and the prediction of the thermodynamic irreversibility by means of an entropy generation analysis is considered. The numerical analysis consider a 3-D CFD model that takes into account the mass transfer, heat transfer, species transport, and electrochemical reactions. Several numerical simulations were performed and each contribution to the local entropy generation rate was computed. The results show different trends of the current density, temperature, species, activation loss, ohmic loss, and concentration loss along the fuel cell. Also, the results show strong variations of the local and global entropy generation rates between the cases analyzed. It is possible to conclude that the fuel cell performance and the prediction of thermodynamic irreversibility can be significantly affected by the choice of the electrochemical models and its parameters, which must be carefully selected.

Key words: *CFD, MOLB-type geometry, electrochemical model parameters, thermodynamic irreversibility, solid oxide fuel*

Introduction

Fuel cells are considered as a promising power generation technology and therefore they have been intensively studied in the last decades. A fuel cell allows a direct conversion of the chemical energy of a fuel into electrical energy by means of electrochemical reactions. Consequently, fuel cells have some advantages compared to the traditional power generation systems [1], such as: high efficiency, fuel flexibility, and low emissions of CO_2, SO_x, and NO_x. Furthermore, fuel cells allow the integration with turbine plants and cogeneration systems [2]. However, some drawbacks such as high costs and durability issues have impeded an extensive diffusion of the fuel cells as a power generation technology. As a result, several research works

* Corresponding author, e-mail: jdj.ramirezminguela@ugto.mx

have been conducted with the aim of improving fuel cells. In particular, many works have focused on the development of efficient and accurate numerical models to simulate solid oxide fuel cells (SOFC).

The CFD models permit a detailed description of both fuel cell geometry and physical phenomena, consequently such numerical techniques have been employed for improving and optimizing fuel cell design. Ferguson *et al*. [3] developed a 3-D SOFC model and they computed temperature, species concentration, and electric potential distribution for various SOFC geometries. Furthermore, this numerical model was used as design tool to obtain optimal values of some fuel cell geometrical parameters. Kulikovsky [4] developed a model for anode performance of a planar-supported SOFC fed by hydrogen. Andersson *et al*. [5] studied the relationships between the electrochemical active area-to-volume ratios, the couplings between the electrochemical activation energies, the current density distribution, and the activation polarizations for an anode-supported planar SOFC in a 3-D numerical model supplying a mixture of hydrogen and steam water as working fuel.

On the other hand, works based on the second-law of thermodynamics have become popular. In particular, entropy generation and exergy analyses have been found effective methods to deal with system performance improvements [6], since these methods provide an insight that can not be achieved by an energy analysis. Several works are available in the literature concerning second-law analysis of fuel cells. However, most of them consider black box models [7-9] and only few works investigate the causes of thermodynamic irreversibility and their local distribution throughout a fuel cell. Calise *et al.* [10] presented a detailed local exergy analysis of a tubular SOFC stack, in particular, a complete parametric analysis was carried out in order to localize the sources and the magnitude of irreversibility along the components of the stack. Then, this analysis was used to detect the parameters to be optimized in order to reduce the overall irreversibility rate in the cell. Rangel-Hernandez *et al*. [11] investigated the entropy generation related to several transport phenomena occurring in a circular proton exchange membrane fuel cell. The authors introduced several dimensionless parameters that allow an easy recognition of the main source of irreversibility and the identification of possible ways of improving fuel cell design. Finally, Li and Faghri [12] proposed design improvements of a direct methanol fuel cell on the basis of entropy generation, which allows a thermodynamic irreversibility decrease.

Although entropy generation analysis has been found to be an effective method, it relies on accurate modeling of physical phenomena and on a proper choice of model parameters. This aspect can be crucial if a second-law analysis is used for improving the performance of SOFC, since such devices are characterized by multi-physics and coupled phenomena.

There are reported several numerical works that use different electrochemical models and parameters, and it should be noted that, to the best of the authors knowledge, there is not a reported work that show the influence of the fuel cell performance due to the variation of the electrochemical model and its parameters in SOFC.

Therefore, a 3-D CFD-based model is developed to evaluate the effects of current density, temperature, activation loss, ohmic loss, and concentration loss distributions along the fuel cell varying the electrochemical model, and its parameters, commonly reported in the literature. In particular, the influence of the exchange current density and electrical conductivity of the electrodes and electrolyte has been studied. The numerical model solves the complex interaction between fluid dynamics and electrochemical kinetics in a MOLB-type geometry SOFC including mass transfer, heat transfer, species transport and electrochemical reactions. It is also used to compute local and global entropy generation rate due to the previosly mentioned phenomena. Four different sets of electrochemical models and parameters are used in order to

investigate how the entropy generation prediction is affected and to highlight the main irreversibility inside of the fuel cell.

Mathematical model formulation

The SOFC geometry

The MOLB-type geometry consists of a trapezoidal cross-section channel for the fuel and air circulation, where the fuel flows along the internal trapezoidal channel, and the air flows along the external channels.

Because of the system geometry, only a part of the fuel cell was modeled and meshed, including one repeating cell unit with a positive-electrolyte-negative, air and fuel channels. The dimensions of the MOLB-type SOFC geometry are depicted in fig. 1 with a length of 100 mm.

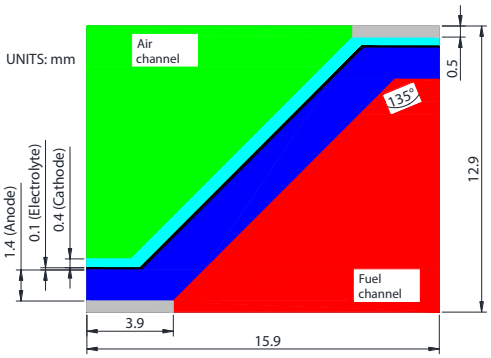

Figure 1. The SOFC: MOLB-type geometry

Electrochemical model

The oxidant reduction reaction takes place in the cathode, where hydrogen is used as fuel, and it is expressed:

$$\frac{1}{2}O_2 + 2e^- \rightarrow O^{2-} \tag{1}$$

The oxygen ions are transferred through the electrolyte and then into the active reaction areas of the anode. The electrochemical reaction of H_2 on anode catalyst is:

$$H_2 + O^{2-} \rightarrow H_2O + 2e^- \tag{2}$$

So, the overall reaction for the SOFC is:

$$H_2 + \frac{1}{2}O_2 \rightarrow H_2O \tag{3}$$

Electrochemical reactions were assumed to occur at the interfaces between the electrodes and the electrolyte [13].

Thermo-fluid model

The model adopted here consists of a set of PDE describing the transport phenomena occurring in the fuel cell [14, 15]. Model parameters are shown in tab. 1. The following assumptions have been adopted: steady-state, incompressible Newtonian ideal gas mixture, homogeneous and isotropic porous media, and thermal equilibrium between solid and gas phases.

Table 1. Model parameters [14, 16]

Porosity [–]	Anode	0.5
	Cathode	0.5
Tortuosity [–]	Anode	3
	Cathode	3
Permeability, [m^2]	Anode	$1.7 \cdot 10^{-10}$
	Cathode	$1.7579 \cdot 10^{-10}$
Thermal conductivity, [$WK^{-1}m^{-1}$]	Anode	6.23
	Cathode	9.6
	Electrolyte	2.7
Density, [kgm^{-3}]	Anode	6200.0
	Cathode	6000.0
	Electrolyte	5560
Specific heat, [$Jkg^{-1}K^{-1}$]	Anode	650
	Cathode	900
	Electrolyte	300

Under the previous assumptions, the equations adopted are, therefore, the continuity equation and the Navier-Stokes equation:

$$\nabla\rho\vec{\nu} = 0 \tag{4}$$

$$\rho(\vec{\nu}\ \nabla)\vec{\nu} = -\nabla p + \mu\nabla^2\vec{\nu} \tag{5}$$

In the porous media, *i. e*. anode and cathode, the continuity eq. (4) and the Darcy-Brinkmann eq. (6) have been used to model the velocity and pressure fields:

$$\rho(\vec{\nu}\ \nabla)\vec{\nu} = -\nabla p + \mu\nabla^2\vec{\nu} - \frac{\mu}{K}\vec{\nu} \tag{6}$$

where K is the permeability of the porous media, $\vec{\nu}$ – the velocity field, p – the pressure, ρ – the density, and μ – the dynamic viscosity. The conservation of each chemical species i have been considered by means of the following transport equations:

$$\nabla(\rho\omega_i\vec{\nu}) = -\nabla\vec{J}_i + S_{o,i} \tag{7}$$

where ω_i is the mass fraction of the i^{th} specie and S_i – the source term due to chemical reaction and is the diffusive flux which is expressed through the Fick's law:

$$\vec{J}_i = -\rho D_{i,\text{eff}}\nabla\omega_i D_{ij} \tag{8}$$

The binary diffusivity, D_{ij}, required to compute $D_{i,\text{eff}}$, is obtained through the Fuller-Schettler-Gidding correlation [17]. In the fuel and air channels, $D_{i,\text{eff}}$, coincides with D_{ij}, while in the porous media, the effective binary diffusivity is computed [18]:

$$D_{i,\text{eff}} = \frac{\varepsilon}{\tau}D_{ij} \tag{9}$$

where ε and τ are the porosity and the tortuosity of the porous media, respectively. Electrochemical reactions take place at the three-phase-boundary (TPB), therefore the source terms S_i are expressed accordingly to Faraday's law:

$$S_i = \begin{cases} \dfrac{j}{n_e F}M_i & \text{TPB} \\ 0 & \text{elsewhere} \end{cases} \tag{10}$$

where M_i is the molar mass of the i^{th} species and is j the current density. The temperature distribution and heat transfer problem is solved by means of the energy equation neglecting viscous effects:

$$\nabla\left[\rho\vec{\nu}\left(h + \frac{\nu^2}{2}\right)\right] = \nabla(k_{\text{eff}}\nabla T - \Sigma_i h_i\vec{J}_i) + S_{o,e} \tag{11}$$

where k_{eff} is the average thermal conductivity of the coexisting solid and gas phases. The source term, S_e, accounts for the ohmic heating, activation losses, and reversible heat due to electrochemical reactions. Ohmic heating takes place in the electrolyte and electrodes, while the other heat source terms are located in the TPB:

$$S_{o,e} = \begin{cases} \dfrac{j^2}{\sigma} + jn_{\text{act}}\dfrac{j}{n_e F}T\Delta S & \text{TPB} \\ 0 & \text{elsewhere} \end{cases} \tag{12}$$

where n_{act} – the activation potential, ΔS – the entropy change associated with the electrochemical reactions, and σ – the electric conductivity. Buttler-Volmer eq. [19] is used for the computation of the current density:

$$j = j_0 \left\{ \exp\left[\frac{\beta n_e F}{\mathrm{R}T} n_{\mathrm{act}} \right] - \exp\left[-\frac{(1-\beta) n_e F}{\mathrm{R}T} n_{\mathrm{act}} \right] \right\} \tag{13}$$

where j_0 is the exchange current density and β – the transfer coefficient. The reversible potential V_{rev} is obtained through the Nernst's equation:

$$V_{\mathrm{rev}} = V^0 + \frac{\mathrm{R}T}{2F} \ln\left(\frac{p_{\mathrm{H_2}} \sqrt{p_{\mathrm{O_2}}}}{p_{\mathrm{H_2O}}} \right) \tag{14}$$

Finally the operating voltage of the fuel cell is given by:

$$V = V_{\mathrm{rev}} - n_{\mathrm{act}} - n_{\mathrm{ohm}} - n_{\mathrm{conc}} \tag{15}$$

where n_{ohm} is the ohimic loss and n_{conc} – the concentration loss.

Local entropy generation rate formulation

Entropy generation quantifies the thermodynamic irreversibility occurring in a system, as a consequence, entropy generation also measures the decrease of available work [20]. According to the second-law of thermodynamics, a reduction of entropy production results in a more efficient system. For this reason, second-law analysis has become a very popular tool to investigate and design efficient energy systems.

Entropy production is due to several mechanisms, such as: heat transfer, mass transfer, and viscous friction [21]. The formulation of the local entropy generation rate is:

$$s_p = \frac{k(\nabla T)^2}{T^2} + \frac{\Delta : \tau}{T} + \sum_i \left(\rho R_i D_i \right) \left(\nabla \omega_i \frac{\Delta X_i}{\Delta X_i} \right) \tag{16}$$

From eq. (16) it is possible to notice that the entropy generation rate is split into three contributions, each one related to a specific transport phenomena:

$$s_p = s_h + s_\mu + s_m \tag{17}$$

The first term of the right hand side is the entropy generation rate due to heat transfer, the second term is the contribution of the viscous stress, and the last one is the entropy generation rate due to mass transfer. In addition, in a fuel cell the entropy production due to ohmic loss must be considered:

$$s_{\mathrm{ohm}} = \frac{1}{T} \left(\frac{j^2}{\sigma} \right) \tag{18}$$

The entropy generation rate due to the activation loss is considered as a surface term:

$$s_{\mathrm{act}} = \frac{j n_{\mathrm{act}}}{T} \tag{19}$$

Finally, the global entropy generation rate over the entire fuel cell for each contribution is obtained:

$$S_i = \int s_i \mathrm{d}V \tag{20}$$

The previous integral is performed over the entire fuel cell domain, and the term s_i is the single contribution, indicated in eqs. (17)-(19).

Cases studied and boundary conditions

Four cases have been considered to investigate the effects of the model parameters. The cases are characterized by different exchange current density and electric conductivity formulations. Table 2 summarizes the models adopted for $j_{0,a}$ and $j_{0,c}$, in Cases I and II, a variable exchange current density has been used, while constant values for $j_{0,a}$ and $j_{0,c}$ have been chosen in Cases III and IV. Furthermore, different pre-exponential coefficients and activation energies have been used for Cases I and II, as reported in tab. 3.

Table 2. Exchange current density formulations [14, 18, 22-25]

	Anode $j_{0,a}$, [Am^{-2}]	Cathode $j_{0,c}$, [Am^{-2}]
Case I and II	$\gamma_a \left(\frac{p_{H_2}}{p_{H_2,\text{ref}}}\right)\left(\frac{p_{O_2}}{p_{O_2,\text{ref}}}\right)\exp\left(-\frac{E_{act,a}}{RT}\right)$	$\gamma_a \left(\frac{p_{O_2}}{p_{O_2,\text{ref}}}\right)^{0.25}\exp\left(-\frac{E_{\text{act},c}}{RT}\right)$
Case III and IV	2300	5300

Table 3. Exchange current density parameters [14, 22, 25]

	Case I	Case II
Anode pre-exponential coefficient, γ_a	$7 \cdot 10^9$	$7 \cdot 10^8$
Cathode pre-exponential coefficient, γ_c	$7 \cdot 10^9$	$5.5 \cdot 10^8$
Anode activation energy $E_{\text{act},a}$, [Jmol^{-1}]	100	110
Cathode activation energy $E_{\text{act},c}$, [Jmol^{-1}]	120	120
Anode transfer coefficient, β	2	2
Cathode transfer coefficient, β	0.6	0.6

Table 4 reports the relations used for the electrical conductivity between electrodes and electrolyte. In the first three cases, a temperature dependent conductivity has been adopted, while in Case IV it has been taken as a constant.

Table 4. Electrical conductivity formulations [14, 18, 22-25]

	Anode σ_a, [Ω^{-1}m^{-1}]	Cathode σ_c, [Ω^{-1}m^{-1}]	Electrolyte σ_e, [Ω^{-1}m^{-1}]
Case I, II and III	$0.00298\exp\left(-\frac{1392}{T}\right)$	$0.008114\exp\left(\frac{500}{T}\right)$	$10\exp\left(\frac{1}{T}-\frac{1}{1273.15}\right)$
Case IV	8261	102191	8.635

Concerning the boundary conditions, a mass flow rate of $4.78 \cdot 10^{-6}$ kg/s is imposed at the anodic fuel cell inlet, while a mass flow rate of $9.18 \cdot 10^{-5}$ kg/s is imposed at the cathode side. Inlet molar fraction of hydrogen is set to 0.49. Fuel inlet temperature is set equal to 973 K, while air enters to the fuel cell at 873 K. Furthermore, ambient pressure is imposed on the outlet cross-sections. Fuel cell is considered to be adiabatic and symmetry boundary conditions are imposed on the left and right planes illustrated in fig. 1. Finally, fuel cell voltage is imposed.

Numerical approach

The transport equations previously illustrated have been solved by means of the commercial finite volume code ANSYS Fluent v 15.0. An iterative algorithm has been implemented through user define functions (UDF) in order to deal with the coupled multi-physics equations previously illustrated, fig. 2. The Navier-Stokes equation and the other transport equations are firstly solved to obtain velocity, temperature, and species concentration distributions. Then, the

local current density is computed and subsequently the local energy and species source terms are updated. The procedure is repeated until convergence is achieved. Finally, the local and global entropy generation rates are calculated and stored. A grid independence study has been performed increasing density and quality from 38 000 up to 1 121 000 cells and a structured mesh of 290 000 cells has been found to be sufficient to achieve grid-independent solutions with a relative error of 1.5 %.

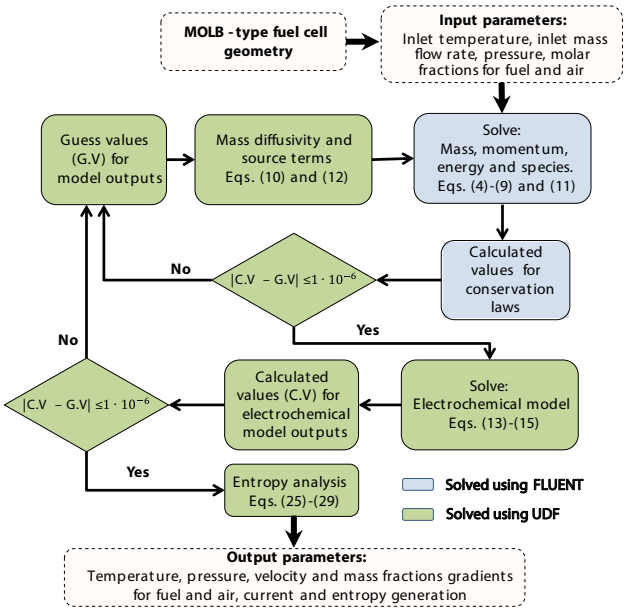

Figure 2. The SOFC model diagram

Results

As illustrated previously, the cases analyzed in this paper differ in the choice of the model parameters. Therefore, it is expected that for a given cell voltage, the net electric power output of the SOFC differs from case to case. However, in order to perform a meaningful comparison, it has been chosen to study the different cases at the same power density. For a given case, this has been achieved by properly tuning the fuel cell voltage until the desired power density was obtained.

Figure 3 illustrates a scattered plot of power density against fuel cell voltage for several simulations performed in this study. Only the marked cases have been compared. As it can be seen, the power density is kept constant and equal to 5800 W/m^2.

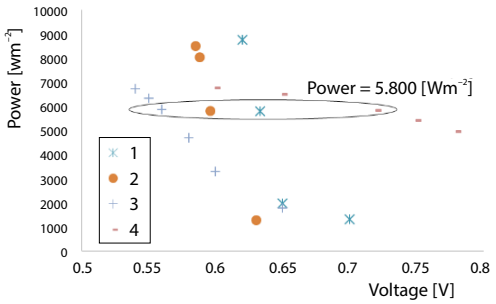

Figure 3. Power density obtained from voltage variation of the cases under study

The computational time required to reach the convergence using a 2.2 GHz CPU with 6 GB in RAM computer for the Case I, II, III, and IV, takes around 14, 12, 3, and 2 hours, respectively. This behavior, particularly in Case I is due to the species concentration dependence of the exchange current density and the temperature dependence of the conductivity, while in the Case IV these values are constants.

The SOFC performance: current density, temperature, and losses distributions

Figure 4 illustrates current density and temperature distributions along the fuel cell and significant differences can be noticed among the four cases. Current density increases along the fuel cell for both Case I and Case II. The behavior is similar since the same formulation of exchange current density and electrical conductivity is used. Only pre-exponential factors and activation energies are different, as reported in tab. 3 in particular, E_{act} at the anodic side is lower

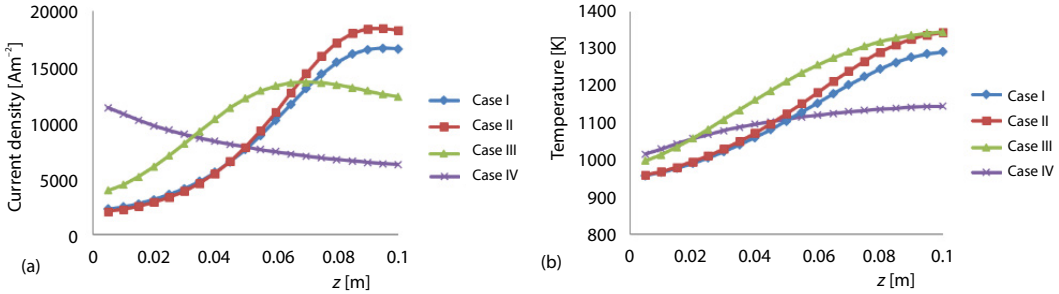

Figure 4. Distribution along the fuel cell; (a) current density, (b) temperature

in Case II. Consequently, current density is higher for z larger than 0.06 m for Case II since temperature is higher near the fuel cell outlet. Current density behavior is strongly affected by the electrodes and electrolyte properties when electric conductivity is modeled as constant (Case IV), current density decreases along the fuel cell. Moreover, the average current density is 12% lower for Case IV compared to Case II. Such behavior is strictly related to the temperature distribution illustrated in fig. 4(b). Electric conductivity is a decreasing function of temperature in Cases I and II; therefore, in such cases ohmic resistance decreases along the fuel cell. As a consequence, the electric current increases along the fuel cell. On the other hand, Case IV is characterized by constant electrical conductivities thus, internal ohmic resistance is not affected by temperature. As a result, the current decreases due to the increase of activation and concentration losses, as illustrated later. The temperature increases along the SOFC, provoked by the heat release due to ohmic heating, activation losses and reversible heat of the electrochemical reactions. As indicated in eq. (12), the heat source terms increase if the current increases, as a result, larger temperatures are obtained for Cases I and II. Case III presents a current density distribution that initially increases and then decreases slightly for z larger than 0.06 m. In such case, electric conductivity is variable, *i. e.* temperature dependent, thus the initial increase of current is again due to a lower ohmic resistance. However, the exchange current density is assumed to be constant, *i. e.* not affected by species concentration and temperature near the fuel cell outlet. As a result, current density near the inlet is larger in Case III compared to Cases I and II, while it does not vary significantly for z larger than 0.06 m.

The voltage losses in each of the cases analyzed are shown in fig. 5. It can be seen that ohmic loss decreases along the fuel cell in Cases I, II, and III, since temperature dependent electrical conductivities are adopted. Ohmic loss is almost constant in Case IV because electrical properties are not affected by temperature. Ohmic loss decreases about 50% along the cell for Cases I and II, which show a very similar behavior. The effect of temperature is even more

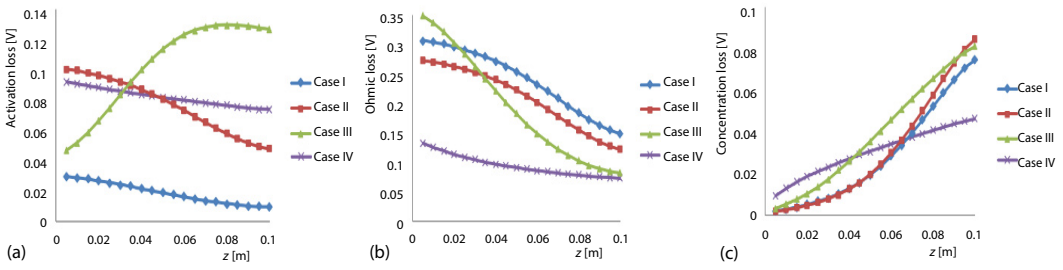

Figure 5. Distribution along the fuel cell; (a) activation loss, (b) ohmic loss, (c) concentration loss

pronounced in Case III, indeed, voltage loss near fuel cell outlet is about one-third of the loss at the inlet region. It can be noticed from fig. 5 that ohmic loss is predominant in all cases: it represents 50% of the overall losses in Case IV and 80% in Case I. The activation loss η_{act} is depicted in fig. 5(a): when constant current density is adopted (Case III) η_{act} it is particularly relevant near fuel cell outlet. As a result, current density is limited for z larger than 0.06 m in Case III, as illustrated in fig. 4(a).

It should be noted that the activation loss in the cases that consider constant exchange current density follow the same tendency of the current density distribution, as it can be observed in fig. 4(a) and fig. 5(a). For case IV, with constant conductivity, the current density decreases throughout the fuel cell, fig. 4(a), the same tendency is observed for the activation loss fig. 5(a). For Case III, with temperature dependent conductivity, the current density increases throughout the fuel cell, fig. 4(a), therefore the activation loss follow the same trend, fig. 5(a).

The concentration loss increases in all the cases along the fuel cell, fig. 5(c) since chemical species are depleted due to the electrochemical reactions. The current density distribution for Case IV differs significantly from the others. Consequently, the concentration loss reported in fig. 5(c) also shows a different behavior. Near the inlet, the current density is larger for Case I, which results in a larger amount of fuel and oxygen depleted and, therefore, the concentration loss is more relevant. The opposite situation occurs at the fuel cell outlet, where current density for Case IV is lower compared to the other cases.

Significant local differences can be also noticed between the cases. Figure 6 depicts hydrogen and oxygen mass fractions at the electrode-electrolyte interfaces for Cases I and IV. Major differences are found in the cross-section at the outlet of the fuel cell: fuel mass fraction is lower for Case I compared to Case IV, especially near the bottom corners. This is related to the different electrical parameters adopted in the two cases. Current density is higher for Case I because of the temperature dependency of the electrical conductivities. The opposite situation occurs near the fuel cell inlet: a larger amount of H_2 is consumed when constant properties are chosen (Case IV) because of a higher current density in the proximity of the fuel entrance. At the cathode side, the major differences are observed along the upper plane of the fuel cell. In this region, oxygen is almost completely depleted for more than half of the fuel cell length if Case I is considered. On the other hand, in Case IV the first half of the fuel cell is predicted to be the more critical one. The concentration loss illustrated in fig. 5(c) is directly related to the species distributions depicted in fig. 6.

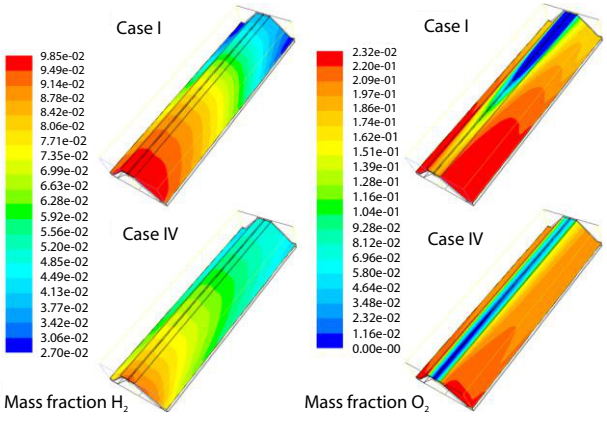

Figure 6. Mass fraction distribution of H_2 and O_2; Case I and Case IV (*for color image see journal web site*)

In Case IV, relevant loss for z larger than 0.06 m is due to the low reactants mass fraction, both at anode and cathode sides of the fuel cell. Such marked differences in the prediction of the species distribution can be particularly important when models are used to investigate upcoming fuel cell design with the aim of avoiding failures due to low reactants concentration.

Entropy generation distributions and the effect of the model parameters on the SOFC

An entropy generation analysis has been performed for the four cases previous considered in order to assess the effect of the model parameters on the prediction of thermodynamic irreversibility. This is a crucial aspect since possible design improvements are based on the results in terms of irreversibility. In order to perform a comparison, the global entropy generation rate has been computed for all the cases. In fig. 7, the specific global entropy generation rates are compared. First of all, it can be observed that the contributions due to the fluid friction are negligible for all the cases. Since fluid-flow in the fuel cell is laminar, viscous stresses are not relevant and the corresponding thermodynamic irreversibility are not significant.

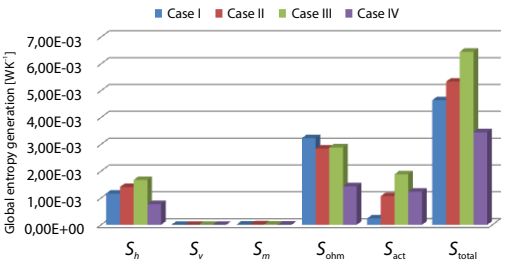

Figure 7. Global entropy generation (*for color image see journal web site*)

The entropy generated due to the heat transfer is comparable to the entropy generated due to the activation loss. However, the major contribution for all the cases is s_{ohm}, that is, entropy production related to the ohmic loss. It can be observed that the larger thermodynamic irreversibility occur in Case III. This case is characterized by a significant entropy production due to the heat transfer and the activation loss. In Case III, constant exchange current density is adopted and, consequently, activation potential η_{act} is higher compared to the other cases as shown in fig. 5(a). As a result, the largest value of the global entropy generation s_{act} occurs in Case III, showing an almost two-fold increase with respect to Case II. The s_{act} is also relevant in Case IV, which further indicates that higher activation loss is predicted when constant exchange current density is adopted.

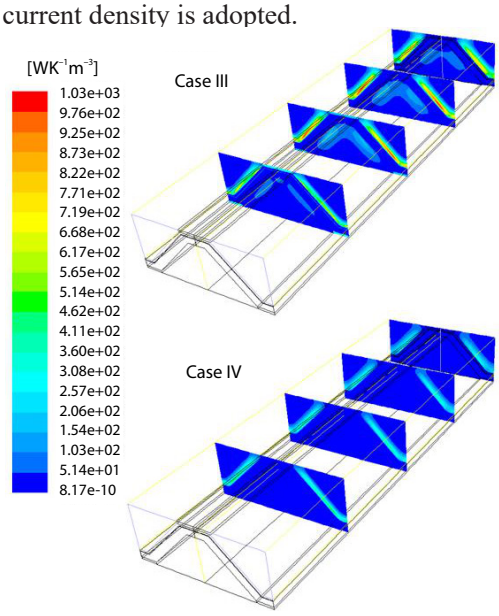

Figure 8. Entropy generation due to the heat transfer; Case III and Case IV (*for color image see journal web site*)

On the other hand s_{act} is not particularly relevant when variable exchange current density is used, in particular in Case I. The minimum value of the global entropy production S_{total} occurs in Case IV, for this case S_{total} is 54% lower compared to Case III. It can be noticed that for Case IV, irreversibility due to the ohmic loss are significantly smaller compared to the other cases because constant electrical conductivity is adopted in every case. Finally, the entropy generation due to the mass transfer s_m is negligible for all the cases.

The entropy generation analysis conducted by CFD, allows one to investigate the local distribution of irreversibility within the system. In fig. 8, the entropy generation due to the heat transfer is depicted for Cases III and IV. For both cases, the entropy generation is located near the electrolyte, since it is here where heat is released because of the electrochemical reactions.

However, it can be noticed that entropy generation due to the heat transfer is less relevant in Case IV compared to Case III. Both the magnitude and the spread of s_h in the cell are larger for Case III, as a consequence, the global entropy generation due to the heat transfer is twice in Case III, compared to Case IV, as illustrated in fig. 7.

Figure 9 illustrates the entropy generation rate due to the activation loss s_{act} along the electrode-electrolyte interface. This kind of irreversibility is predominant in Case III and it increases from the inlet to the middle section of the SOFC. In Case IV, the activation entropy generation rate shows the opposite trend, the entropy production is more relevant near the inlet and it decreases along the fuel cell. Moreover, the magnitude of s_{act} is larger for Case III. As a result, Case III shows the highest global irreversibility due to the activation as pointed out in fig. 7.

The entropy generation due to the ohmic loss is depicted in fig. 10. This contribution is only present in the solid conductive components, *i. e.* electrodes and electrolyte. It can be immediately noticed that local value of s_{ohm} is up to one order of magnitude higher that the contributions shown in figs. 8 and 9. As a result, this kind of irreversibility is the most relevant, as it is also reported in fig. 7. However, the distribution of s_{ohm} in Case III differs significantly from Case IV. The entropy generation due to the ohmic loss decreases along the fuel cell in Case IV, since the current density shows the same behavior, fig. 4, and constant electrical conductivities are adopted. On the other hand, s_{ohm} increases from fuel cell inlet to the middle part of the cell, where the highest irrevesibility are found when temperature dependent properties are used (Case III).

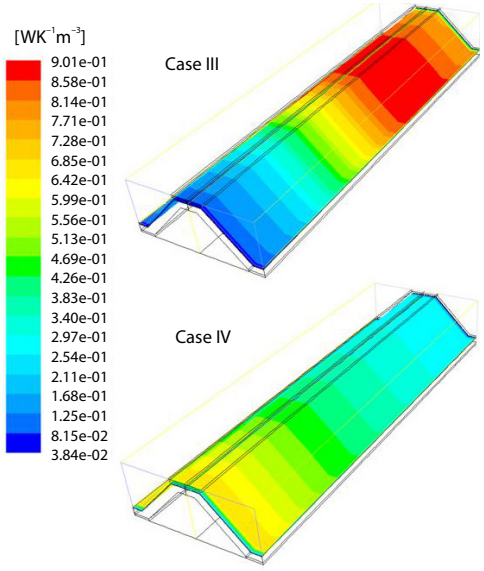

Figure 9. Entropy generation due to activation loss; Case III and Case IV (*for color image see journal web site*)

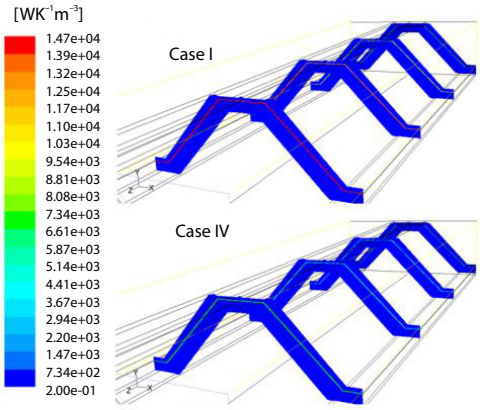

Figure 10. Entropy generation due to ohmic loss; Case III and Case IV (*for color image see journal web site*)

Conclusions

In this work, the effect of varying the electrochemical model and its parameters for a SOFC has been assessed. In particular, the influence of the exchange current density and the electrical conductivity of the electrodes and electrolyte have been studied. The numerical analysis is based on a 3-D CFD model that takes in account the mass transfer, heat transfer, species transport, and electrochemical reactions. Besides, a second-law analysis of the SOFC has been performed. The entropy generation contributions due to fluid friction, heat transfer, mass transfer, ohmic heating, and activation losses have also been considered. The analysis indicates that:

- The choice of the electrochemical model and its parameters affect significantly the computational time of convergence, mainly due to the species concentration dependency on the exchange current density.
- Numerical predictions of fuel cell behavior are strongly influenced by the exchange current density and electrical conductivity adopted in the model. Current density decreases along the fuel cell when electrical conductivity is assumed to be constant. On the other hand when a temperature dependent electrical conductivity is used, current density increases along the fuel cell because of a reduction of the ohmic resistance. Exchange current density mainly affects the activation loss: if a constant exchange current density is adopted the model predicts higher activation loss.
- The numerical prediction of thermodynamic irreversibility shows relevant variations if different model parameters are used. When a variable electrical conductivity is used, the global entropy generation shows about a two-fold increase compared to the case with constant electrical properties. The major contribution to the overall irreversibility is always due to the ohmic heating, which can account up to 70% of the total entropy generation. Nevertheless, its contribution strongly depends on the selected model. The entropy production due to heat transfer and activation loss is comparable. However, the activation entropy production is predicted to be more significant when a constant exchange current density is used in the model. Finally, the entropy generation contributions due to mass transfer and viscous effects are not relevant in the SOFC configuration. As a result, from this analysis it can be stated that the prediction of the thermodynamic irreversibility are significantly affected by the choice of the electrochemical model parameters. This is a key aspect if entropy generation is used to improve the performance of a SOFC.

Acknowledgment

The authors are grateful to the University of Guanajuato, the Programa para el Desarrollo Profesional Docente (PRODEP), Folio-UGTO-PTC-477, DSA/103.5/15/7007, and the Consejo Nacional de Ciencia y Tecnologia (CONACYT) for their financial support.

Nomenclature

D_{ij} – mass diffusion coefficient, [m^2s^{-1}]
$D_{i,\text{eff}}$ – effective mass diffusion coefficient, [m^2s^{-1}]
E_{act} – activation energy cathode, [$Jmol^{-1}$]
F – Faraday constant, [96,487 $Cmol^{-1}$]
$\vec{J}_i$ – diffusive flux of species i, [$kgm^{-2}s^{-1}$]
j – current density, [Am^{-2}]
j_0 – exchange current density, [Am^{-2}]
k – thermal conductivity, [$Wm^{-1}K^{-1}$]
k_{eff} – thermal effective conductivity, [$Wm^{-1}K^{-1}$]
M_i – molecular weight of the species i [kg mol^{-1}]
n_e – number of electrons, [–]
n_{act} – activation potential, [V]
n_{ohm} – ohmic loss, [V]
n_{conc} – concentration loss, [V]
p – pressure, [Pa]
R – universal gas constant, [$Wmol^{-1}K^{-1}$]
S_i – global entropy generation rate, [WK^{-1}]
$S_{o,e}$ – energy source term, [$Wm^{-3}s^{-1}$]
$S_{o,i}$ – species source term, [$kgm^{-3}s^{-1}$]
S_h – heat transfer entropy generation rate, [$WK^{-1}m^{-3}$]
s_m – mass transfer entropy generation rate, [$WK^{-1}m^{-3}$]
s_p – entropy generation rate, [$WK^{-1}m^{-3}$]
s_μ – fluid friction entropy generation rate, [$WK^{-1}m^{-3}$]
T – temperature, [K]
$\vec{v}$ – velocity, [ms^{-1}]
V – voltage, [V]
X_i – molar fraction of species i

Greek symbols

β – transfer coefficient
γ – pre-exponential factor
Δ – strain tensor, [s^{-1}]
ε – porosity, [–]
μ – viscosity, [ms^{-2}]
ρ – density, [kgm^{-3}]
σ – electrical conductivity, [$\Omega^{-1}m^{-1}$]
τ – tortuosity [-]
ω_i – mass fraction of species i

References

[1] Subhash, C., Singhal, K. K., *High Temperature Solid Oxide Fuel Cells: Fundamentals, Design and Applications*, Elsevier Ltd, Amsterdam, Netherlands, 2003
[2] Massardo, A. F., Lubelli, F., Internal Reforming Solid Oxide Fuel Cell-Gas Turbine Combined Cycles (IRSOFC-GT): Part A – Cell Model and Cycle Thermodynamic Analysis, *Journal of Engineering for Gas Turbines and Power*, *122* (2000), 1, pp. 27-35
[3] Ferguson, J. R., *et al*., Three-Dimensional Numerical Simulation for Various Geometries of Solid Oxide Fuel Cell, *Journal of Power Sources*, *58* (1996), 2, pp. 109-122
[4] Kulikovsky, A. A., *et al*., A Model for SOFC Anode Performance, *Electrochemica Acta*, *54* (2009), 26, pp. 6686-6695
[5] Andersson, M., *et al*., Three Dimensional Modeling of an Solid Oxide Fuel Cell Coupling Charge Transfer Phenomena with Transport Processes and Heat Generation, *Electrochim Acta, 109* (2013), Oct., pp. 881-893
[6] Kaushik, S. C., *et al*., Energy and Exergy Analyses of Thermal Power Plants: A Revie, *Renewable and Sutainable Energy Reviews*, *15* (2011), 4, pp. 1857-1872
[7] Calise, F., *et al*., Simulation and E xergy Analysis of a Hybrid Solid Oxide Fuel Cell (SOFC) – Gas Turbine System, *Energy*, *31* (2006), 15, pp. 3278-3299
[8] Naterer, G. F., *et al*., Fuel Cell Entropy Production with Ohmic Heating and Diffusive Polarization, *International Journal of Heat and Mass Transfer*, *49* (2006), 15-16, pp. 2673-2683
[9] Baniasadi, E., Dincer, I., Energy and Exergy Analyses of a Combined Ammonia-Fed Solid Oxide Fuel Cell System for Vehicular Applications, *International Journal of Hydrogen Energy*, *36* (2011), 17, pp. 11128-11136
[10] Calise, F., *et al*., Parametric Exergy Analysis of a Tubular Solid Oxide Fuel Cell (SOFC) Stack through Finite-Volume Mode, *Applied Energy*, *86* (2009), 11, pp. 2401-2410
[11] Rangel-Hernandez, V. H., *et al*., Entropy Generation Analysis of a Proton Exchange Membrane Fuel Cell (PEMFC) with a Fermat Spiral as a Flow Distributo,. *Energy*, *36* (2011), 8, pp. 4864-4870
[12] Li, X., Faghri, A., Local Entropy Generation Analysis on Passive High-Concentration DMFCs (Direct Methanol Fuel Cell) with Different Cell Structures, *Energy*, *36* (2011), 1, pp. 403-414
[13] Gorte, R. J., Recent Developments Towards Commercialization of Solid Oxide Fuel Cell, *AIChE J*., *51* (2005), 9, pp. 2238-377
[14] Bove, R., Ubertini, S., Modeling Solid Oxide Fuel Cell Operation: Approaches, Techniques and Results, *Journal of Power Sources*, *159* (2006), 1, pp. 543-559
[15] Bird, R. B., *et al*., *Transport Phenomena*, John Wiley & Sons, New York, USA, 1960
[16] Costamagna, P., Honegger, K., Modeling of Solid Oxide Heat Exchanger Integrated Stacks and Simulation at High Fuel Utilization, *J. Electrochem. Soc*., *145* (1998), 11, pp. 3995-4007
[17] Bird, R. B., *et al*., Transport Phenomena, Reverte, S. A., 1992
[18] Chan, S. H., *et al*., A Complete Polarization Model of a Solid Oxide Fuel Cell and its Sensitivity to the Change of Cell Components Thickness, *Journal of Power Sources*, *93* (2001), 1-2, pp. 130-140
[19] P. J. Gellings, H. J. M. Bouwmeester, Ed., *Handbook of Solid State Electrochemistry*, CRC Press, Boca Raton, Fla, USA, 1997, pp. 269-294 and pp. 407-480
[20] Bejan, A., *Advanced Engineering Thermodynamics*, John Wiley and Sons, New York, USA, 2006
[21] De Groot, S. R., Mazur, P., *Non-Equilibrium Thermodynamics*, Dover Publications, New York, USA, 2011
[22] Campanari, S., Iora, P., Definition and Sensitivity Analysis of a Finite Volume SOFC Model for a Tubular Cell Geometry, *Journal of Power Sources*, *132* (2004), 1/2, pp. 113-126
[23] Pei-Wen, L., Minking K. C., Simulation of the Chemical/Electrochemical Reactions and Heat/Mass Transfer for a Tubular SOFC in a Stack, *J. of Power Sources*, *124* (2003), 2, pp. 487-498
[24] Yunzhen, Y., *et al*., Comparison of Heat and Mass Transfer between Planar and MOLB-Type SOFCs, *J. Power Sources*, *177* (2008), 2, pp. 426-433
[25] Yuzhang, W., *et al*., Numerical Investigation of DifferentsLload Effect on the Performance of Planar Electrode Supported SOFC with Syngas as Fuel, *I*., *J. Hydrogen Energy*, *36* (2011), 9, pp. 5624-5631

Paper submitted: December 21, 2015
Paper revised: May 20, 2017
Paper accepted: May 20, 2017